Laser-Induced Phosphorescence of SO_2 in Solid Neon: Direct Observation of the $\tilde{b}^3A_2$ State in the $^{16}OS^{18}O$ Molecule

Ching-Chi Zen, I-Chia Chen, and Yuan-Pern Lee*,†

Department of Chemistry, National Tsing Hua University, 101, Sec. 2, Kuang Fu Road, Hsinchu, Taiwan 30013

A. J. Merer

Department of Chemistry, The University of British Columbia, 2036 Main Mall, Vancouver, B. C., Canada V6T 1Z1

Received: September 14, 1999; In Final Form: November 5, 1999

Laser excitation of isotopically labeled SO_2 molecules in a neon matrix has allowed the measurement of dispersed phosphorescence spectra ($\tilde{a}^3B_1$-$\tilde{X}^1A_1$) in the wavelength region 387.5−526.3 nm (19 000−25 800 cm^{-1}). The origin of the $\tilde{a}-\tilde{X}$ transition lies at 25 747 cm^{-1} in $^{16}OS^{16}O$, shifted 18 cm^{-1} to the red from the gas phase; the three vibrational frequencies of the $\tilde{X}$ state are nearly unperturbed in the neon matrix (1149, 520, and 1362 cm^{-1}). As the zero-phonon lines are sharp and well resolved, it has been possible to monitor emission from a specific isotopomer to obtain its excitation spectrum. The excitation spectra of matrix-isolated $^{16}OS^{16}O$ and $^{18}OS^{18}O$ in the region 350.9−388.5 nm (25 740−28 500 cm^{-1}) are similar to those previously observed in the gas phase, with strong perturbations affecting all vibrational levels above $\tilde{a}^3B_1(110)$ at 27 005 cm^{-1} (370 nm). Two additional groups of bands are observed for the unsymmetrical isotopomer $^{18}OS^{16}O$; they are identified as transitions to levels of the $\tilde{a}^3B_1$ state with $\upsilon_3 = 1$ and as direct transitions to the $\tilde{b}^3A_2$ state, which both become allowed in the lower symmetry. The ν_3 frequency of the $\tilde{a}^3B_1$ state of $^{18}OS^{16}O$ is 922 cm^{-1}; for the $\tilde{b}^3A_2$ state, $\nu_1 \simeq 791$ cm^{-1} and $\nu_2 \simeq 315$ cm^{-1}, while the $\tilde{b}$ (001) level lies 26 653 cm^{-1} above the $\tilde{X}$ (000) level.

I. Introduction

The electronic transitions of SO_2 in the UV region are exceptionally complicated and have attracted continued interest over the years.[1−20] The longest wavelength transition is the $\tilde{a}^3B_1-\tilde{X}^1A_1$ system, which begins at 388 nm. Its first few vibrational bands, up to the $\tilde{a}(100)-\tilde{X}(000)$ band at 370 nm, are regularly spaced and nearly unperturbed rotationally.[3,6,20] Beyond this point the structure becomes progressively more disorganized. Extra vibrational features appear and the spacings of the bands are irregular. Analysis of the gas-phase spectrum at high resolution[20] shows that the principal irregularities are caused by another triplet state, which can be identified as $\tilde{b}^3A_2$. The interaction between the two states becomes increasingly severe at shorter wavelength, to the extent that the spectrum is almost unassignable by 357 nm, where the $\tilde{A}^1A_2-\tilde{X}^1A_1$ transition begins.[14]

Detailed rotational analysis of the perturbed $\tilde{a}^3B_1$ levels near 370 nm by Hallin et al.[20] has revealed the pattern of the antisymmetric vibrational levels of the $\tilde{b}^3A_2$ state and shows that the lowest level, $\tilde{b}^3A_2(001)$, lies near 26 700 cm^{-1}. The presence of this perturbing triplet state has been invoked to explain the vibrational anharmonicity,[4,6] the phosphorescence quenching,[21,22] and some aspects of the photochemistry[23−25] of SO_2 in this region. Ab initio calculations indicate that a third triplet state, $\tilde{c}^3B_2$, may lie nearby,[26,27] but there is no experimental evidence for its location. Snow et al.[28] have observed phosphorescence of crystalline SO_2 at 4.2 K originating 83 cm^{-1} below the (000) level of the $\tilde{a}^3B_1$ state; they have assigned it to a new triplet state, but no direct observation of this state has yet been reported for isolated SO_2. The gas-phase results indicate that the (000) level of the $\tilde{b}^3A_2$ state lies 300 ± 100 cm^{-1} above the (000) level of the $\tilde{a}^3B_1$ state, which suggests that the phosphorescence observed by Snow et al.[28] may come from the $\tilde{b}^3A_2$ state, shifted considerably below the $\tilde{a}^3B_1$ state in the pure solid.

Laser-induced emission from a matrix provides several advantages for detecting unknown electronic transitions.[29−32] Because the relaxation pathways and selection rules for species in a matrix are often different from those in the gas phase, one may be able to observe states that are inaccessible in the gas phase. Emission accompanying recombination reactions of photofragments trapped in a matrix cage may also originate from a state that is difficult to access in the gas phase. In this work we demonstrate a further advantage of laser-induced emission from a matrix. By selectively monitoring the zero-phonon line (ZPL) in the $^{16}OS^{18}O$ phosphorescence, we have observed additional excitation lines that were not seen in $^{16}OS^{16}O$ and $^{18}OS^{18}O$; the extra lines become allowed in the lower symmetry of the unsymmetrical isotopomer and are identified as lines associated with the ν_3 vibrations of the $\tilde{a}^3B_1$ and $\tilde{b}^3A_2$ states.

II. Experimental Details

The experimental apparatus is similar to that described previously.[30−32] The matrix support was a gold-plated copper mirror maintained at 5 K. Matrix samples were prepared by

* Corresponding author. Fax (886) 35 722892. E-mail: yplee@mx.nthu.edu.tw.

† Jointly appointed by the Institute of Atomic and Molecular Sciences, Academia Sinica, Taipei, Taiwan.

10.1021/jp9932517 CCC: $19.00
Published on Web 01/04/2000

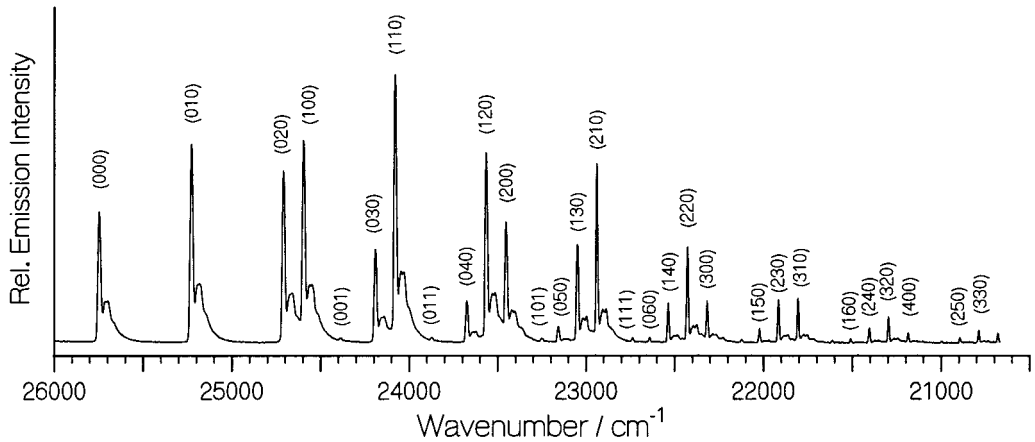

Figure 1. Laser-induced phosphorescence spectra of a matrix sample with $S^{16}O_2$/Ne = 1/2000; excitation wavelength 370.22 nm, slit width 0.15 mm, gate width 2 ms. The vibrational assignments refer to the lower state ($\tilde{X}^1A_1$).

depositing a premixed gaseous mixture of SO_2 in Ne (volumetric ratio Ne/SO_2 = 2000) onto the matrix support. Typically 2−5 mmol of mixture was deposited over a period of 1 h.

The matrix was irradiated with light from a dye laser (350−390 nm, ∼4 mJ/pulse) pumped by a XeCl excimer laser (10 Hz). The emission was spectrally resolved with a 0.64-m monochromator (Jobin-Yvon, 1200 grooves mm^{-1}, reciprocal linear dispersion 1.2 nm mm^{-1}) before being detected with a photomultiplier (Hamamatsu R212UH). The signal was subsequently amplified (bandwidth 5 MHz) before being sent to a boxcar integrator (EG&G, models 4402 and 4420). The signal was typically averaged over 30 laser pulses for each data point. The monochromator was typically stepped at 0.04-nm increments for phosphorescence measurement, using slit widths of 0.1−0.2 mm. For the excitation scans, the monochromator was set to a specific wavelength, with slit widths of 0.15−0.2 mm, and the dye laser was stepped at 0.02-nm increments. The estimated uncertainty in the wavelength measurements is ±0.04 nm for sharp ZPL phosphorescence lines.

SO_2 (99.98%) was used without further purification except for degassing at 77 K. $^{18}OS^{18}O$, with nominal isotopic purity of 98%, and $^{16}O^{34}S^{16}O$ (isotopic purity 93.15%) were obtained from Cambridge Isotope Laboratories; $^{16}OS^{18}O$ was produced by isotopic exchange of a mixture of $^{16}OS^{16}O$ and $^{18}OS^{18}O$.

III. Results and Discussion

A. Dispersed Phosphorescence of SO_2 in Solid Ne. Figure 1 shows the dispersed phosphorescence spectrum of $S^{16}O_2$ isolated in solid Ne at 5 K upon laser excitation at 370.29 nm (27 006 cm^{-1}); the figure covers the region 384.6−487.8 nm (20 500−26 000 cm^{-1}). Excitation at other resonant wavelengths in the region 350−388 nm produces identical spectra, indicating that vibrational relaxation is facile in this matrix. The emission lines exhibit narrow ZPL with fwhm of about 5 cm^{-1} and relatively small phonon wings. Phosphorescence spectra reported previously for solid SO_2 and for SO_2 isolated in Ar, Kr, SF_6, and other hosts show much enhanced phonon wings that prevent accurate measurements of the line positions in the various progressions.[4,28,33] In our spectra, the vibrational progressions are well resolved, and weak progressions involving odd quanta of ν_3'' are recorded for the first time.

Emission spectra of $^{18}OS^{18}O$ and $^{16}O^{34}S^{16}O$ show similar vibrational patterns to that of $^{16}OS^{16}O$. Because the ZPL lines are narrow, we could excite $^{16}OS^{18}O$ selectively and observe its emission spectrum free from interference by the $^{16}OS^{16}O$ or $^{18}OS^{18}O$ molecules that were also present in the matrix sample. The measured wavenumbers of the emission lines of these four isotopomers of SO_2 are listed in Table 1. To our knowledge, information on $^{16}OS^{18}O$ has not been reported.

The assignments of the lower state vibrational quantum numbers are unambiguous. The observed frequencies of ν_1 = 1149, ν_2 = 520, and ν_3 = 1362 cm^{-1} are nearly identical to those of $^{16}OS^{16}O$ in the gas phase (1151.4, 517.7, and 1361.8 cm^{-1})[34−38] and in an Ar matrix (1152, 520, and 1355 cm^{-1}).[39−41] The line positions have been fitted to the standard equation

$$\nu = A - \sum_i \omega_i\left(\nu_i + \frac{1}{2}\right) - \sum_{j\geq i} x_{ij}\left(\nu_i + \frac{1}{2}\right)\left(\nu_j + \frac{1}{2}\right) \quad (1)$$

where A is the energy of the zero point level of the $\tilde{a}^3B_1$ state. The derived vibrational constants of the four isotopomers of SO_2 are listed in Table 2. Two sets of anharmonic constants are given in this table; the second set, in parentheses, is from a fit to a reduced data set where the levels involving ν_3'' were omitted. In a Ne matrix, the electronic origin ν_{00} of the $\tilde{a}-\tilde{X}$ system of $^{16}OS^{16}O$ shifts by only 18 cm^{-1} (<0.1%) to the red relative to the gas phase. In general, the vibrational levels of the $\tilde{X}^1A_1$ state of SO_2 are nearly unperturbed by the Ne host.

B. Excitation Spectra of SO_2 in Solid Ne. The excitation spectrum shown as trace A of Figure 2 was recorded by monitoring the emission of $^{16}OS^{16}O$ at 396.46 ± 0.18 nm (25 223 cm^{-1}), corresponding to the $\tilde{a}(000)\rightarrow\tilde{X}(010)$ band, and stepping the laser at 0.02-nm increments in the spectral range 350.9−384.6 nm (26 000−28 500 cm^{-1}). The spectrum is not normalized to the output intensity of the dye laser. The vibrational assignments in Figure 2 refer to the upper state because only the (000) level of the electronic ground state is populated in matrix-isolation experiments. The vibrational pattern is similar to that reported for the gas phase.[6] The level spacings behave normally up to the $\tilde{a}^3B_1(110)$ band at 27 005 cm^{-1}. The five intense features with irregular spacings above 27 200 cm^{-1} are assigned to the (200), (002), (210), (012), and (300) levels of the $\tilde{a}^3B_1$ state, respectively, based on the gas-phase results.[6,12,13,20] Weak bands at 28 121 and 28 247 cm^{-1} can be assigned as transition to the $\tilde{a}(220)$ and $\tilde{a}(022)$ levels, and the band at 28 485 cm^{-1} is assigned to $\tilde{a}(102)$. The irregular vibrational spacings result from the interaction of the $2\nu_1$ and $2\nu_3$ levels of the $\tilde{a}^3B_1$ state, which lie close in energy.

The excitation spectra of $^{18}OS^{18}O$ and $^{16}O^{34}S^{16}O$ shown in traces C and D of Figure 2 were recorded with isotopically pure samples; the monochromator was set to the $\tilde{a}(000)\rightarrow\tilde{X}(010)$ and $\tilde{a}(000)\rightarrow\tilde{X}(110)$ bands, respectively (395.91 ± 0.18 and 415.11

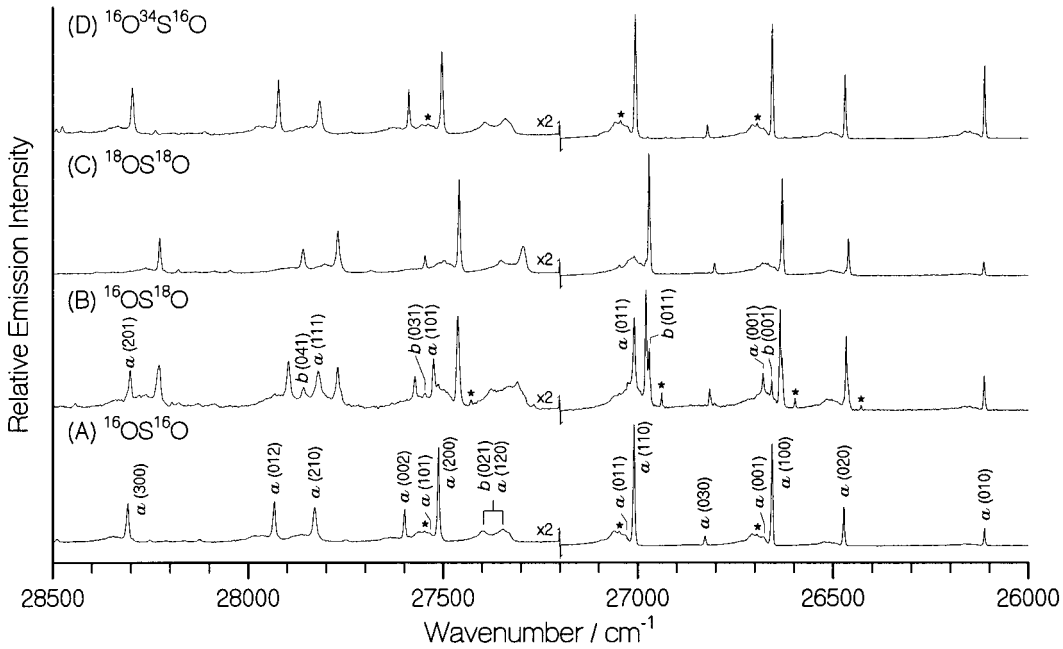

Figure 2. Laser excitation spectra of various isotopomers of SO_2 in the region 26 000−28 500 cm^{-1}. The vibrational assignments refer to the upper state because only the $\tilde{X}(000)$ level is initially populated. (A) $^{16}OS^{16}O$, probed at 396.46 nm (25 223 cm^{-1}), slit width 0.15 mm; (B) $^{16}OS^{18}O$, probed at 396.17 nm (25 242 cm^{-1}), slit width 0.12 mm (only lines additional to those in (A) are marked); (C) $^{18}OS^{18}O$, probed at 395.91 nm (25 258 cm^{-1}), slit width 0.15 mm; (D) $^{16}O^{34}S^{16}O$, probe at 415.11 nm (24 090 cm^{-1}), slit width 0.2 mm. Lines marked with * are due to a distinct matrix site.

± 0.24 nm). The vibrational patterns are very similar to that of $^{16}OS^{16}O$. Observed line positions of various isotopomers of SO_2 are listed in Table 3.

Pure $^{16}OS^{18}O$ cannot be prepared because of rapid isotopic exchange between ^{16}O and ^{18}O. However, because the ZPLs of the phosphorescence are sharp, we could monitor a specific wavelength region where emission from $^{16}OS^{18}O$ dominates and thereby obtain excitation spectra of $^{16}OS^{18}O$ free from interference by other species. Trace B of Figure 2 is the excitation spectrum recorded when the $\tilde{a}(000) \rightarrow \tilde{X}(010)$ line of $^{16}OS^{18}O$ at 396.17 ± 0.15 nm (25 242 cm^{-1}) was monitored. The main features correspond to those of the symmetric isotopomers, but the excitation spectrum also shows numerous new lines.

These additional lines can become allowed either because the symmetry is lower in $^{16}OS^{18}O$, or because new relaxation pathways open as a result of different relative energy orders of certain levels following isotopic substitution. Since all upper states are observed to have lifetimes of about 14 ms in the Ne matrix, and also since no new bands are observed in dispersed emission, the second reason is unlikely.

With the lowered symmetry in $^{16}OS^{18}O$ the ν_3 vibration becomes totally symmetric, so that $\Delta v_3 = \pm 1$ bands are no longer forbidden in the $\tilde{a}-\tilde{X}$ transition. At the same time $\tilde{a}^3B_1$ and $\tilde{b}^3A_2$ states both become $^3A''$, so that vibronic coupling can occur through all three vibrations, not just ν_3. Additional interactions between $\tilde{a}$ and $\tilde{b}$ states therefore become possible.

C. Direct Observation of $\tilde{a}(v_1v_21) \leftarrow \tilde{X}(000)$ Transitions. Two extra lines of $^{16}OS^{18}O$ are found at 26 653 and 26 676 cm^{-1}, near the $\tilde{a}(100) \leftarrow \tilde{X}(000)$ band; these lie 899 and 922 cm^{-1} above the origin at 25 754 cm^{-1}, respectively. It is likely that the ν_3 vibration of the $\tilde{a}^3B_1$ state is involved in these new bands because the ν_3 frequency of $^{16}OS^{16}O$ has been variously estimated[12,13] to lie between 907 and 984 cm^{-1}. Observation of a Coriolis (vibration−rotation) perturbation at low K in the $\tilde{a}(100)$ level shows that the $\tilde{a}(001)$ level actually lies 927 ± 2 cm^{-1} above the $\tilde{a}(000)$ level.[20] From a normal-mode analysis, the isotopic shift for the ν_3 mode of $^{16}OS^{18}O$ should be about 6 cm^{-1}; therefore it seems fairly certain that the band at 26 676 cm^{-1} is the $\tilde{a}(001) \leftarrow \tilde{X}(000)$ transition. With this assignment the vibrational frequency ν_3 of matrix-isolated $^{16}OS^{18}O$ is given as 922 cm^{-1}, with a possible uncertainty of ±2 cm^{-1}. The alternative assignment of 26 653 cm^{-1} to the $\tilde{a}(001) \leftarrow \tilde{X}(000)$ band implies an unreasonably large matrix shift for ν_3; hence it is unlikely.

A value of ν_3 can be estimated also from isotope shifts of the electronic origin. The isotope shift of the origin is given approximately by

$$\Delta\nu = \frac{1}{2}\sum_{k=1}^{3}[(\nu'_k - \nu''_k) - (\nu'_k(i) - \nu''_k(i))] \qquad (2)$$

in which ν and $\nu(i)$ refer to the normal and the substituted isotopomers. Taking the bond angle in the $\tilde{a}^3B_1$ state as 126.1°, we calculate that the ratio $\nu'_3(i)/\nu'_3$ should be 0.9658; this leads to the value $\nu'_3 = 880 \pm 90$ cm^{-1}, which is consistent with our assignment.

A new band of $^{16}OS^{18}O$ at 27 005 cm^{-1} can be assigned as $\tilde{a}(011) \leftarrow \tilde{X}(000)$, since it lies one quantum of ν'_2 above the $\tilde{a}(001)-\tilde{X}(000)$ band. To be exact, the separation of the bands is 329 cm^{-1}, slightly less than the $\tilde{a}(010)-\tilde{a}(000)$ interval of 356 cm^{-1}, but consistent with the expected anharmonicity. This assignment is also consistent with the Coriolis perturbation found at K = 11−12 in the high-resolution gas-phase spectra[6,20] of $^{16}OS^{16}O$.

Bands at 27 519 and 27 815 cm^{-1} are readily assigned as transitions to the $\tilde{a}(101)$ and $\tilde{a}(111)$ levels of $^{16}OS^{18}O$; they lie between the mixed (200)/(002) and (210)/(012) pairs, respectively. The spacing of 296 cm^{-1} between these bands is also consistent with a vibrational quantum of ν_2. Similarly, the band at 28 124 cm^{-1}, 309 cm^{-1} above the $\tilde{a}(111) \leftarrow \tilde{X}(000)$ band, can be assigned as $\tilde{a}(121) \leftarrow \tilde{X}(000)$. The relatively intense band at 28 295 cm^{-1} is assigned as a transition to the $\tilde{a}(201)$ state; the interval of 776 cm^{-1} between the $\tilde{a}(201)$ and $\tilde{a}(101)$ levels,

TABLE 1: Observed Wave Numbers (cm^{-1}) of $\tilde{a}^3B_1(000)-\tilde{X}^1A_1(v_1''v_2''v_3'')$ Phosphorescence for Various Isotopomers of SO_2

$(v_1''v_2''v_3'')$	$^{16}OS^{16}O$	$^{16}OS^{18}O$	$^{18}OS^{18}O$	$^{16}O^{34}S^{16}O$
(0 0 0)	25 743	25 750	25 756	25 746
(0 1 0)	25 223	25 242	25 258	25 230
(0 2 0)	24 706	24 733	24 761	24 715
(0 3 0)	24 189	24 226	24 265	24 204
(0 4 0)	23 671	23720	23 769	23 690
(0 5 0)	23 153	23 213	23 274	23 177
(0 6 0)	22 639	22 706	22 778	22 666
(0 7 0)	22 120	22 200	22 286	
(0 8 0)	21 609		21 786	
(0 9 0)	21 101		21 296	
(0 10 0)	20 594			
(1 0 0)	24 594	24 626	24 654	24 603
(1 1 0)	24 075	24 121	24 160	24 090
(1 2 0)	23 562	23 617	23 668	23 578
(1 3 0)	23 046	23 111	23174	23 070
(1 4 0)	22 532	22 607	22 680	22 560
(1 5 0)	22 018	22 105	22 187	
(1 6 0)	21 507	21 603	(21 696)	
(1 7 0)	20 997	21 100	(21 206)	
(1 8 0)	20 486			
(1 9 0)	(19 985)[a]			
(2 0 0)	23 448	23 511	23 562	23 465
(2 1 0)	22 935	23 008	23 070	(22 965)
(2 2 0)	22 423	22 505	22 577	22 451
(2 3 0)	21 912	22 002	22 089	21 943
(2 4 0)	21 401	21 501	21 600	21 435
(2 5 0)	20 891	21 000	21 107	
(2 6 0)	20 382			
(2 7 0)	19 880			
(2 8 0)	(19 379)			
(3 0 0)	22 313	22 397	22 476	22 338
(3 1 0)	21 802	21 904	21 987	21 831
(3 2 0)	21 294	21 404	21 500	21 326
(3 3 0)	20 785	20 905	21 012	20 825
(3 4 0)	20 279			
(3 5 0)	19 770			
(3 6 0)	(19 258)			
(4 0 0)	21 183		21 396	21 213
(4 1 0)	20 678		20 911	20 712
(4 2 0)	20 174			
(4 3 0)	19 668			
(4 4 0)	19 164			
(5 0 0)	20 061			
(5 1 0)	19 561			
(5 2 0)	19 060			
(0 0 1)	24 381	24 416	24 440	24 413
(0 1 1)	23 868		23 948	23 891
(1 0 1)	23 247		23 355	23 270
(1 1 1)	22 734		22 861	22 764
(1 2 1)	22 226		22 370	

[a] Values in parentheses are not included in the fitting.

68 cm^{-1} smaller than that for the previous members of the ν_1 progression, is consistent with the anharmonicity observed for the $(v_1 00)$ progression.

Based on a normal-mode analysis, the ν_3 values of $^{16}OS^{16}O$, $^{18}OS^{18}O$, and $^{16}O^{34}S^{16}O$ are estimated to be about 926, 897, and 921 cm^{-1}, respectively. With these estimates, we are able to locate a few weak $\tilde{a}(v_1v_21) \leftarrow \tilde{X}(000)$ bands for $^{16}OS^{16}O$, $^{18}OS^{18}O$, and $^{16}O^{34}S^{16}O$, as listed in parentheses in Table 3. These weak bands are overlapped with phonon wings of the more intense $\tilde{a}(v_1+1v_21) \leftarrow \tilde{X}(000)$ bands; hence the assignments are less certain.

D. Direct Observation of $\tilde{b}(v_1v_21) \leftarrow \tilde{X}(000)$ Transitions in $^{16}OS^{18}O$. The new band of $^{16}OS^{18}O$ at 26 653 cm^{-1} mentioned in the previous section must arise from a different electronic state because all of the possible $\tilde{a}^3B_1$ levels in this region have been identified. The analysis of the rotational perturbations in the gas-phase spectra[20] places the $\tilde{b}^3A_2(001)$ level about 37 cm^{-1} above the $\tilde{a}^3B_1(100)$ level in $^{16}OS^{16}O$. As the band at 26 653 cm^{-1} lies 20 cm^{-1} above the $\tilde{a}(100) \leftarrow \tilde{X}(000)$ band, it is therefore logical to assign this band of $^{16}OS^{18}O$ as the $\tilde{b}^3A_2(001) \leftarrow \tilde{X}^1A_1(000)$ band, appearing directly in absorption.

In principle the $\tilde{b}(001) \leftarrow \tilde{X}(000)$ band should appear weakly in the spectrum of a symmetrical isotopomer (such as $^{16}OS^{16}O$) but, as Figure 2 shows, it is perhaps overlapped with the $\tilde{a}(100) \leftarrow \tilde{X}(000)$ band near 26 651 cm^{-1} for $^{16}OS^{16}O$ and $^{16}O^{34}S^{16}O$, and lost under the phonon wings of the $\tilde{a}(100) \leftarrow \tilde{X}(000)$ band of $^{18}OS^{18}O$. With the lower symmetry of $^{16}OS^{18}O$ the situation is different. As we saw in the previous section, the close-lying ν_1 and ν_3 vibrational levels of the $\tilde{a}$ state are both totally symmetric, so that the $\tilde{a}(001) \leftarrow \tilde{X}(000)$ band becomes allowed by the vibrational selection rules. In addition, the $\tilde{b}(001)$ level can interact directly with the close-lying $\tilde{a}(001)$ level since their vibration−electronic wave functions both transform as A'' in the C_s point group. The interaction transfers intensity to the $\tilde{b}(001) \leftarrow \tilde{X}(000)$ band, with the result that three bands now appear in this region of the spectrum.

A similar pattern of bands is found near the position of the $\tilde{a}(110) \leftarrow \tilde{X}(000)$ band of $^{16}OS^{18}O$ at 26 976 cm^{-1}. The peak at 27 005 cm^{-1}, to the high-energy side of the strong $\tilde{a}(110)-\tilde{X}(000)$ band, is immediately assigned as $\tilde{a}(011) \leftarrow \tilde{X}(000)$, which can appear in the lower symmetry molecule because the upper state is vibrationally totally symmetric. This confirms the assignment presented in the previous section. The third peak at 26 968 cm^{-1}, which lies just to the red of the $\tilde{a}(110) \leftarrow \tilde{X}(000)$ band, can be assigned as a direct transition to the $\tilde{b}^3A_2(011)$ level. The assignment is consistent with the gas-phase results[20] for $^{16}OS^{16}O$ which shows that there is a strong vibronic perturbation at very low K in the $\tilde{a}^3B_1(110)$ level. In the gas phase, the $\tilde{b}(011)$ level lies a few cm^{-1} above the $\tilde{a}(110)$ level for $^{16}OS^{16}O$, but the energy order is reversed for $^{16}OS^{18}O$ in the Ne matrix. The vibrational frequency of ν_2 for the $\tilde{b}(001)$ state of $^{16}OS^{18}O$ is thus determined to be 315 cm^{-1}, consistent with the estimate of $\nu_2 \sim 300$ cm^{-1} from the gas-phase results.[20]

The bands at 27 343 and 27 394 cm^{-1} in $^{16}OS^{16}O$, and their counterparts in the other isotopomers, are surprisingly broad. The gas-phase spectrum in this region shows a doubled band,[4,6] whose upper states are shown by high-resolution analysis[20] to be 50:50 mixtures of the interacting $\tilde{a}^3B_1(120)$ and $\tilde{b}^3A_2(021)$ levels. Perhaps such a strong mixing involves active phonon coupling, hence the ZPL are diminished. The relative intensity of these two broad bands varies among the different isotopomers, presumably because the interaction between $\tilde{a}(120)$ and $\tilde{b}(021)$ depends on their relative energies. The band at 27 394 cm^{-1} has a relatively large red shift (28 cm^{-1}) from the gas phase as compared with other bands (17−21 cm^{-1}), indicating that the interaction is stronger in the matrix and this level is pushed down further.

The $\tilde{b}(101)$ level lies close to the $\tilde{a}(200)$ level according to results in the gas phase.[20] We do not observe any additional band near the $\tilde{a}(200)-\tilde{X}(000)$ band of $^{16}OS^{18}O$ at 27 457 cm^{-1}. Hence, it is likely that the weak $\tilde{b}(101)-\tilde{X}(000)$ band is overlapped with the $\tilde{a}(200)-\tilde{X}(000)$ band; such an assignment implies a value ~ 804 cm^{-1} for the ν_1 vibration, consistent with the estimate of 780 cm^{-1} in the gas phase. Further support comes from the observation of a shoulder at 27 759 cm^{-1} on the $\tilde{a}(210)-\tilde{X}(000)$ band of $^{16}OS^{18}O$ at 27 765 cm^{-1}. If the shoulder is assigned as the $\tilde{b}(111)-\tilde{X}(000)$ band, it implies intervals of 302 and 791 cm^{-1} from the $\tilde{b}(101)$ and $\tilde{b}(011)$ levels, respectively, consistent with the observed ν_2 and ν_1 frequencies.

The newly observed weak lines of $^{16}OS^{18}O$ at 27 543, 27 853,

TABLE 2: Vibrational and Anharmonicity Constants (in cm^{-1}) of the $\tilde{X}^1A_1$ States of Various Isotopic Species of SO_2 Isolated in Solid Ne[a]

level	$^{16}OS^{16}O$ gas[b]	$^{16}OS^{16}O$ Ne	$^{16}OS^{18}O$ Ne	$^{18}OS^{18}O$ Ne	$^{16}O^{34}S^{16}O$ Ne
ν_1	1151.4	1149	1124	1102	1143
ν_2	517.7	520	508	498	516
ν_3	1361.8	1362	1334	1316	1333
ω_1	1166.6	1170.0 ± 1.4 (1161.0 ± 1.5)[c]	1140.0 ± 1.7 (1133.0 ± 1.7)[c]	1116.0 ± 2.0 (1110.0 ± 1.5)[c]	1155.5 ± 2.5 (1150.0 ± 1.8)[c]
ω_2	522.0	526.3 ± 0.9 (524.0 ± 1.3)	512.7 ± 0.8 (510.9 ± 0.8)	500.2 ± 0.8 (499.1 ± 0.7)	517.5 ± 1.9 (517.0 ± 1.4)
ω_3	1378.5	1384.9 ± 2.3	1354.1 ± 2.0	1332.0 ± 2.1	1349.4 ± 3.5
$-x_{11}$	3.71	4.0 ± 0.1 (3.9 ± 0.2)	3.7 ± 0.4 (3.7 ± 0.4)	3.6 ± 0.2 (3.7 ± 0.3)	3.5 ± 0.3 (3.1 ± 0.3)
$-x_{22}$	0.34	0.55 ± 0.04 (0.63 ± 0.06)	0.26 ± 0.08 (0.26 ± 0.08)	0.20 ± 0.05 (0.20 ± 0.06)	0.38 ± 0.20 (0.30 ± 0.20)
$-x_{33}$	4.39	5.17[d]	5.17[d]	5.17[d]	5.17[d]
$-x_{12}$	3.03	3.4 ± 0.1 (4.5 ± 0.2)	3.1 ± 0.2 (3.1 ± 0.2)	3.0 ± 0.2 (2.9 ± 0.2)	3.4 ± 0.3 (3.1 ± 0.3)
$-x_{13}$	12.94	16.5 ± 1.6	14.8[d]	13.1 ± 1.5	6.8 ± 2.1
$-x_{23}$	4.12	6.2 ± 1.1	4.2[d]	2.2 ± 0.9	−0.5 ± 2.0

[a] The error limits represent one standard deviation. [b] References 34−38; see also ref 38 for fitted parameters including y_{ijk} terms. [c] Values in parentheses are from a second fit in which data for the ν''_3 levels were not included. [d] Values without error limits are constrained in the fitting.

TABLE 3: Observed Wave Numbers/cm^{-1} of the $\tilde{a}^3B_1$ - $\tilde{X}^1A_1$ Excitation Spectra for Various Isotopic Species of SO_2

$^{16}OS^{16}O$	$^{16}OS^{18}O$	$^{18}OS^{18}O$	$^{16}O^{34}S^{16}O$	assignment
25 747	25 754	25 763	25 750	***a*** (000)
26 109	26 110	26 111	26 109	***a*** (010)
26 470	26 463	26 457	26 466	***a*** (020)
26 651	26 633	26 626	26 651	***a*** (100)
	26 653			***b*** (001)
(26 672)[a]	26 676	(26 657)	(26 674)[a]	***a*** (001)
26 823	26 811	26 800	26 817	***a*** (030)
	26 968			***b*** (011)
27 005	26 976	26 968	27 002	***a*** (110)
	27 005			***a*** (011)
27 174	27 158	27 134		***a*** (040)
	27 263			?
27 343[b]	27 303[b]	27 291[b]	27 337[b]	***a*** (120)/***b*** (021)
	(27 327)			***a*** (021)?
27 394[b]	27 370[b]	27 348[b]	27 387[b]	***b*** (021)/***a*** (120)
27 507	27 457	27 454	27 500	***a*** (200)
(27 532)	27 519	(27 493)	(27 519)	***a*** (101)
	27 543			***b*** (031)
27 594	27 566	27 543	27 583	***a*** (002)
27 748?	27 725?	27 681	27 735	***a*** (130)?
	27 759			***b*** (111)
27 826	27 765	27 766	27 813	***a*** (210)
	27 815			***a*** (111)
	27 853			***b*** (041)
27 928	27 891	27 856	27 917	***a*** (012)
28 121	28 080	28 040	28 105	***a*** (220)
(28 158)	28 124	(28 082)		***a*** (121)?
28 207		28 131	28 186	?
	28 172			***b*** (051)
28 247	28 191	28 173	28 232	***a*** (022)
28 303	28 225	28 221	28 291	***a*** (300)
	28 295	(28 256)		***a*** (201)?
28 485	28 438	28 380	28 471	***a*** (102)

[a] Small peaks overlapped by the phonon wings of other bands are listed in parentheses. [b] Broad band without ZPL.

and 28 172 cm^{-1} can then be assigned as a continuation of the bending progression $\tilde{b}^3A_2(0v'_2\ 1) - \tilde{X}(000)$ with $v'_2 = 3-5$. The observed spacings corresponding to the ν_2 vibrational intervals of the $\tilde{b}^3A_2$ state of $^{16}OS^{18}O$ are in the range 302−319 cm^{-1}.

The transition origins and vibrational frequencies of the $\tilde{a}$ and $\tilde{b}$ states of the various isotopomers of SO_2 isolated in solid Ne are summarized in Table 4; they are also compared with the values for $^{16}OS^{16}O$ in the gas phase. The $\tilde{a}$ state is red-shifted by ∼18 cm^{-1} in the Ne matrix, with vibrational

TABLE 4: Transition Origins and Vibrational Wave Numbers (in cm^{-1}) of the $\tilde{a}^3B_1$ and $\tilde{b}^3A_2$ States of Various Isotopomers of SO_2 Isolated in Solid Ne

state	ν_i	$^{16}OS^{16}O$ gas[a]	$^{16}OS^{16}O$ Ne	$^{16}OS^{18}O$ Ne	$^{18}OS^{18}O$ Ne	$^{16}O^{34}S^{16}O$ Ne
$\tilde{a}^3B_1$	(000)	25 765.7	25 747	25 754	25 763	25 750
	ν_1	906.4	904	879	863	901
	ν_2	360.6	362	356	348	359
	ν_3	927 ± 2	(927)[b]	922	(895)[b]	(924)[b]
$\tilde{b}^3A_2$	(001)			26 653		
	(011)	27 030.8		26 968		
	ν_1	∼780		791[c]		
	ν_2	∼300		315[d]		
	ν_3	∼700				

[a] From refs 6 and 20. [b] Values in parentheses are less certain because they are based on small peaks overlapped by phonon wings. [c] From the $\tilde{b}^3A_2(011)$ level; the (101) level is overlapped with the $\tilde{a}(200)$. [d] From the $\tilde{b}^3A_2(001)$ level.

frequencies nearly unpertubed. Our experiments provide direct observation of bands involving the ν_3 vibration of the $\tilde{a}$ state. Direct observation of bands associated with excitation to various levels of the $\tilde{b}^3A_2$ state are also consistent with estimates based on perturbations in the gas phase. The $\tilde{b}$ state is estimated to be red-shifted by more than 40 cm^{-1}, reversing the order for some levels of the $\tilde{a}$ and $\tilde{b}$ states, as discussed previously.

IV. Conclusion

In this paper we demonstrate an advantage offered by laser-induced emission spectroscopy of species isolated in a matrix. By selectively monitoring the sharp ZPL of the $\tilde{a} - \tilde{X}$ phosphorescence of the unsymmetrical isotopomer $^{16}OS^{18}O$ isolated in solid Ne, we have observed additional lines which have no analogues in the excitation spectra of the symmetrical species $^{16}OS^{16}O$, $^{18}OS^{18}O$, or $^{16}O^{34}S^{16}O$. These lines are assigned as progressions involving odd quantum of ν_3 in the $\tilde{a}^3B_1$ state, together with transitions to the $\tilde{b}^3A_2$ state. The direct observation of these lines of $^{16}OS^{18}O$ enables us to show that the false origin of the $\tilde{b}(001) \leftarrow \tilde{X}(000)$ transition may lie at 26 653 cm^{-1} and that the ν_1 and ν_2 frequencies are about 791 and 315 cm^{-1}, respectively, for $^{16}OS^{18}O$. Direct observation of bands involving ν_3 of the $\tilde{a}$ state yields $\nu_3 = 927$ cm^{-1} for $^{16}OS^{16}O$, confirming the gas-phase value based on rotational perturbations.

Acknowledgment. We thank the National Science Council of the Republic of China for support (project no. NSC 89-2119-M-007-001) and the Ministry of Education, Taiwan, for support of this collaborative research between Canada and Taiwan.

References and Notes

(1) Clements, J. H. *Phys. Rev.* **1935**, *47*, 224.
(2) Metropolis, N.; Beutler, H. *Phys. Rev.* **1940**, *57*, 1078.
(3) Merer, A. J. *Discuss. Faraday Soc.* **1963**, *35*, 127.
(4) Hochstrasser, R. M.; Marchetti, A. P. *J. Mol. Spectrosc.* **1970**, *35*, 335.
(5) Brand, J. C. D.; Jones, V. T.; di Lauro, C. *J. Mol. Spectrosc.* **1971**, *40*, 616.
(6) Brand, J. C. D.; Jones, V. T.; di Lauro, C. *J. Mol. Spectrosc.* **1973**, *45*, 404.
(7) Kent, J. E.; O'Dwyer, M. F.; Shaw, R. J. *Chem. Phys. Lett.* **1974**, *24*, 221.
(8) Tinti, D. S. *Chem. Phys. Lett.* **1971**, *12*, 169.
(9) Hallin, K. E. J.; Hamada, Y.; Merer, A. J. *Can. J. Phys.* **1976**, *54*, 2118.
(10) Wampler, F. B.; Oldenborg, R. C.; Rice, W. W. *J. Appl. Phys.* **1979**, *50*, 6117.
(11) Al-Adel, F.; Hamdan, A.; Binbrek, O.; Baskin, J. S. *Chem. Phys. Lett.* **1992**, *189*, 23.
(12) Baskin, J. S.; Al-Adel, F.; Hamdan, A. *Chem. Phys.* **1995**, *200*, 181.
(13) Joens, J. A. *Chem. Phys. Lett.* **1996**, *261*, 659.
(14) Hamada, Y.; Merer, A. J. *Can. J. Phys.* **1974**, *52*, 1443.
(15) Hamada, Y.; Merer, A. J. *Can. J. Phys.* **1975**, *53*, 2555.
(16) Hegazi, E.; Al-Adel, F.; Hamdan, A.; Dastageer, A. *J. Phys. Chem.* **1994**, *98*, 12169.
(17) Rassias, G.; Metha, G. F.; McGilvery, D. C.; Morrison, R. J. S.; O'Dwyer, M. F. *J. Mol. Spectrosc.* **1997**, *181*, 78.
(18) Al-Adel, F.; Hegazi, E.; Dastageer, A.; Hamdan, A. *Mol. Phys.* **1997**, *90*, 225.
(19) Shaw, R. J.; Kent, J. E.; O'Dwyer, M. F. *J. Mol. Spectrosc.* **1980**, *82*, 1.
(20) Hallin, K. E. J.; Hamada, Y.; Merer, A. J., to be published.
(21) Sidebottom, H. W.; Badcock, C. C.; Calvert, J. G.; Reinhardt, G. W.; Rabe, B. R.; Damon, E. K. *J. Am. Chem. Soc.* **1971**, *93*, 2587.
(22) James, F. C.; Kerr, J. A.; Simons, J. P. *Chem. Phys. Lett.* **1974**, *25*, 431.
(23) Cehelnik, E.; Spicer, C. W.; Heicklen, J. *J. Am. Chem. Soc.* **1971**, *93*, 5371.
(24) Chung, K. J.; Calvert, J. G.; Bottenheim, J. W. *Int. J. Chem. Kinet.* **1975**, *7*, 161.
(25) Heicklen, J.; Kelly, N.; Partymiller, K. *Rev. Chem. Intermediates* **1980**, *3*, 315 and references therein.
(26) Hillier, I. H.; Saunders, V. R. *Mol. Phys.* **1971**, *22*, 193.
(27) Katagiri, H.; Sako, T.; Hishikawa, A.; Yazaki, T.; Onda, K.; Yamanouchi, K.; Yoshino, K. *J. Mol. Struct.* **1994**, *413*−*414*, 589.
(28) Snow, J. B.; Hovde, D. C.; Colson, S. D. *J. Chem. Phys.* **1982**, *76*, 3956.
(29) Bondybey, V. E. In *Chemistry and Physics of Matrix-isolated Species*; North-Holland: Amsterdam, 1989; p 107−137.
(30) Chiang, S.-Y.; Lee, Y.-P. *J. Chem. Phys.* **1988**, *89*, 13.
(31) Zen, C.-C.; Tang, F.-T.; Lee, Y.-P. *J. Chem. Phys.* **1992**, *96*, 8054.
(32) Hung, W.-C.; Ho, C.-D.; Liu, C.-P.; Lee, Y.-P. *J. Phys. Chem.* **1996**, *100*, 3927.
(33) Meyer, B.; *Low Temperature Spectroscopy*; Elsevier: New York, 1971; and references therein.
(34) Flaud, J. M.; Perrin, A.; Salah, L. M.; Lafferty, W. J.; Guelachlvili, G. *J. Mol. Spectrosc.* **1993**, *160*, 272.
(35) Shelton, R. D.; Nielsen, A. H.; Fletcher, W. H. *J. Chem. Phys.* **1953**, *21*, 2178.
(36) Brand, J. C. D.; Humphrey, D. R.; Douglas, A. E.; Zanon, I. *Can. J. Phys.* **1973**, *51*, 530.
(37) Hoy, A. R.; Brand, J. C. D. *Mol. Phys.* **1978**, *36*, 1409.
(38) Yamanouchi, K.; Takeuchi, S.; Tsuchiya, S. *J. Chem. Phys.* **1990**, *92*, 4044.
(39) Sodeau, J. R.; Lee, E. K. C. *J. Phys. Chem.* **1980**, *84*, 3358.
(40) Maillard, D.; Allavena, M.; Perchard, J. P. *Spectrochim. Acta* **1975**, *31A*, 1523.
(41) Chen, L.-S.; Lee, C.-I.; Lee, Y.-P. *J. Chem. Phys.* **1996**, *105*, 9454.